

Measurements of the momentum and current transport from tearing instability in the Madison Symmetric Torus reversed-field pinch^{a)}

A. Kuritsyn,^{1,2,b)} G. Fiksel,^{1,2} A. F. Almagri,^{1,2} D. L. Brower,^{2,3} W. X. Ding,^{2,3} M. C. Miller,^{1,2} V. V. Mirnov,^{1,2} S. C. Prager,^{1,2} and J. S. Sarff^{1,2}

¹Department of Physics, University of Wisconsin, Madison, Wisconsin 53706, USA

²Center for Magnetic Self-Organization in Laboratory and Astrophysical Plasmas, University of Wisconsin-Madison, Madison, Wisconsin 53706, USA

³Department of Physics, University of California, Los Angeles, California 90095, USA

(Received 7 December 2008; accepted 9 February 2009; published online 4 May 2009)

In this paper measurements of momentum and current transport caused by current driven tearing instability are reported. The measurements are done in the Madison Symmetric Torus reversed-field pinch [R. N. Dexter, D. W. Kerst, T. W. Lovell, S. C. Prager, and J. C. Sprott, *Fusion Technol.* **19**, 131 (1991)] in a regime with repetitive bursts of tearing instability causing magnetic field reconnection. It is established that the plasma parallel momentum profile flattens during these reconnection events: The flow decreases in the core and increases at the edge. The momentum relaxation phenomenon is similar in nature to the well established relaxation of the parallel electrical current and could be a general feature of self-organized systems. The measured fluctuation-induced Maxwell and Reynolds stresses, which govern the dynamics of plasma flow, are large and almost balance each other such that their difference is approximately equal to the rate of change of plasma momentum. The Hall dynamo, which is directly related to the Maxwell stress, drives the parallel current profile relaxation at resonant surfaces at the reconnection events. These results qualitatively agree with analytical calculations and numerical simulations. It is plausible that current-driven instabilities can be responsible for momentum transport in other laboratory and astrophysical plasmas. © 2009 American Institute of Physics. [DOI: 10.1063/1.3090325]

I. INTRODUCTION

The physics of intrinsic plasma rotation and momentum transport is of interest in both laboratory and astrophysical plasmas. In many cases rotation is observed even in the absence of externally applied torques. It is also observed that the rate of the radial momentum transport can greatly exceed that predicted from classical collisional viscosity. A widely accepted premise is that the flow is driven by fluctuation-induced stresses (Maxwell and Reynolds) caused by an instability. The specific nature of the instability can vary depending on the type of plasma. For example, while the cause of intrinsic plasma rotation in a tokamak is not yet fully understood,¹ it is nonetheless believed that the flow is driven by electrostatic fluctuations.² Plasma rotation in the reversed-field pinch (RFP) in the absence of discrete magnetic reconnections is attributed to electrostatic fluctuations as well.^{3,4} In astrophysical accretion disks, the rapid radial transport of angular momentum is believed to be caused by flow driven magnetorotational instability.⁵

Magnetic fluctuations have been long considered as a plausible candidate for explaining energy, particle, and current transport in various magnetic confinement configurations.^{6–9} In the RFP, magnetic field is strongly sheared and multiple resonance surfaces exist across the minor radius at locations where the safety factor $q(r) = rB_\phi / RB_\theta$ is a rational number m/n , where m is poloidal and n is toroidal mode

number. In the Madison Symmetric Torus (MST) RFP multiple tearing modes are spontaneously excited at the resonant surfaces during global reconnection events,^{10–12} which give rise to the fluctuation-induced electromotive forces (EMFs) affecting current dynamics. These EMFs, also called magnetohydrodynamic^{13–16} (MHD) and Hall^{17–19} dynamos, lead to relaxation and flattening of the parallel current density profile in MST.^{20,21}

The plasma in the MST RFP rotates spontaneously, and this rotation abruptly changes during repetitive bursts of tearing fluctuations that cause magnetic field reconnection.^{22,23} Thus, another mechanism of momentum transport—fluctuation-induced stresses from current-driven tearing instability—can exist. Prior measurements made in the MST RFP found that momentum transport is anomalous and that it is strongly enhanced by the nonlinear coupling of multiple tearing modes.^{23,24}

In this paper we provide new experimental evidence for momentum transport driven by tearing instability. We present measurements that illustrate the parallel flow profile flattening during the reconnection events. We also present detailed local measurements of fluctuation-induced Maxwell and Reynolds stresses in the plasma edge and the core that drive this relaxation (in the core, only the Maxwell stress has been measured). A surprising result is that both stresses are large and oppositely directed, and their net balance is approximately equal to the plasma acceleration. In addition, it is shown that momentum dynamics is closely coupled to the current dynamics. The fluctuation-induced Maxwell stress enters Ohm's law as the Hall dynamo. Both Hall dynamo and Maxwell stress are shown to be large at the resonant surfaces

^{a)}Paper JII 6, *Bull. Am. Phys. Soc.* **53**, 120 (2008).

^{b)}Invited speaker. Corresponding author. Electronic mail: kuritsyn@wisc.edu. Present address: Cymer, Inc., San Diego, CA, 92127, USA.

during reconnection events and are responsible for driving electric current and plasma flow, respectively. We also provide additional evidence that the multiple global reconnections are imperative for momentum transport. The previous experiments demonstrated that momentum transport is small during reconnection events in the nonreversed RFP plasma with only the core modes being resonant.²³ Here, we have shown that momentum transport also remains small for the case of reversed plasma, where both core and edge modes are resonant, but only the core resonant modes are large, while the edge modes are small.

The article is organized as follows. In Sec. II a short summary of two-fluid relaxation theory is presented. In Sec. III MST experimental setup and measurement techniques are described. Section IV reports measurements of the fluctuation-induced Hall dynamo. In Sec. V measurements of the momentum transport and fluctuation-induced forces are presented. Section VI contains discussion and Sec. VII provides conclusions.

II. PLASMA RELAXATION IN RFP

A. Current profile relaxation

Current profile flattening is one of the key predictions of Taylor's relaxation theory—under an assumption of global helicity conservation the plasma state with the minimum energy has a uniform j_{\parallel}/B profile, where B is the magnetic field and j_{\parallel} is the current density component parallel to the magnetic field.²⁵ Likewise, three-dimensional resistive MHD simulations show that when the magnetic fluctuations are larger, the current profile is flatter,¹³ a trend consistent with Taylor's conjecture. The experimentally measured dynamics of the current profile evolution in MST agrees with this prediction—the current profile flattens at the reconnection event.^{20,21}

The driving forces for these phenomena have been associated with the fluctuation-induced intrinsic EMF or dynamo. The generation and sustaining of the mean field-aligned electric current is present in many laboratory and astrophysics plasmas. In particular, it is known that in the RFP the simple Ohm's law is not satisfied ($E \neq \eta j$) in the discharges with large magnetic fluctuations and that some noninductive current drive mechanism must exist.^{15,26} It is especially evident in the vicinity of the RFP reversal surface, where the magnetic field and the plasma current become almost entirely poloidal while the externally applied inductive electric field has only the toroidal component. Moreover, the electric field and field-aligned current are antiparallel in the plasma edge during global reconnection events.

In the framework of the two-fluid MHD, the current dynamics are governed by the generalized Ohm's law that can be written in the form²⁷

$$\mathbf{E} + \mathbf{v} \times \mathbf{B} = \eta \mathbf{j} + \frac{\mathbf{j} \times \mathbf{B}}{ne} - \frac{\nabla P_e}{ne} - \frac{m_e d\mathbf{v}_e}{e dt}. \quad (1)$$

Here, \mathbf{E} is the electric field, \mathbf{B} is the magnetic field, \mathbf{j} is the total current density, P_e is the electron pressure, \mathbf{v} is the ion fluid velocity, \mathbf{v}_e is the electron fluid velocity, n is the plasma density, η is the plasma resistivity, m_e is the electron mass,

and e is the electron charge. The last three terms on the right hand side (RHS) of Eq. (1), the Hall term, gradient of the electron pressure, and electron inertia represent the two-fluid effects beyond the standard MHD description. It has been recently theoretically demonstrated that two-fluid physics play an important role during magnetic reconnection process^{28,29} and the Hall effect has been experimentally observed in the magnetospheric³⁰ and laboratory³¹ current sheets.

After representing each of the quantities in Eq. (1) as a sum of its mean value and a nonaxisymmetric fluctuating component (denoted by the tilde), averaging over a magnetic flux-surface (denoted by $\langle \dots \rangle$), and taking the component parallel to the equilibrium magnetic field, the parallel mean-field Ohm's can be written as¹⁴

$$\eta j_{\parallel} = E_{\parallel} + \langle \tilde{\mathbf{v}} \times \tilde{\mathbf{B}} \rangle_{\parallel} - \frac{1}{ne} \langle \tilde{\mathbf{j}} \times \tilde{\mathbf{B}} \rangle_{\parallel}, \quad (2)$$

where $j_{\parallel} = \langle j_{\parallel} \rangle$ is the mean current density and $E_{\parallel} = \langle E_{\parallel} \rangle$ is the mean parallel electric field. The second term on the RHS is the fluctuation-induced MHD dynamo and the third term is the Hall dynamo. Here, the electron inertia term has been neglected because it is small, and the parallel pressure gradient term has vanished upon the flux-surface averaging.

The MHD dynamo was measured in Refs. 15, 16, and 32 and was found to be significant in the core as well as at the periphery of the plasma. However, it was shown in Ref. 16 to be small in the vicinity of the reversal surface, suggesting that other effects, in particular, the fluctuation-induced Hall dynamo, may be important. Indeed, later experimental measurements of the Hall dynamo in the core of the RFP plasma by laser Faraday rotation diagnostic found that it is significant at the $q=1/6$ resonant surface.^{18,19} In this paper, we show the Hall dynamo to be large at the edge, near the reversal surface, during reconnection.

B. Two-fluid relaxation

Single-fluid Taylor relaxation theory has been generalized for the two-fluid (ion and electron) case.^{33,34} The two-fluid relaxation theory assumes that electron and ion helicities are conserved separately. It predicts that the minimum energy (fully relaxed) state corresponds to the field-aligned electrical current and plasma momentum (normalized to the mean magnetic field) that are constant across the plasma radius,

$$j_{\parallel}/B = \lambda_1, \quad (3)$$

and

$$nV_{\parallel}/B = \lambda_2. \quad (4)$$

Equation (3) represents the relaxation of the parallel current profile first described by Taylor²⁵ and has been reviewed above. Similarly, Eq. (4) describes the relaxation of the parallel plasma momentum profile.

The parallel momentum balance equation can be represented in a fashion similar to the parallel Ohm's law [Eq. (2)],

$$\rho \frac{\partial V_{\parallel}}{\partial t} = \langle \tilde{\mathbf{j}} \times \tilde{\mathbf{B}} \rangle_{\parallel} - \rho \langle \tilde{\mathbf{V}} \cdot \nabla \tilde{\mathbf{V}} \rangle_{\parallel}. \quad (5)$$

Here, the term on the left hand side is the ion inertia ($V_{\parallel} = \langle V_{\parallel} \rangle$ is the mean parallel velocity, $\rho = \langle \rho \rangle$ is the mass density). The terms on the RHS are the fluctuation-induced Maxwell and Reynolds stresses, respectively. The pinch term $\langle \tilde{\rho} \tilde{V}_r \rangle \partial V_{\parallel} / \partial r$ and terms associated with pressure, viscosity, etc., are estimated to be small and have been omitted.

It is of importance that the Maxwell stress also contributes to the dynamics of the plasma parallel electric current by entering the mean-field parallel Ohm's law as the Hall dynamo term $\langle \tilde{\mathbf{j}} \times \tilde{\mathbf{B}} \rangle_{\parallel} / (ne)$. This suggests that the dynamics of the parallel electric current and the parallel plasma flow are closely coupled. Analytical calculations and MHD numerical simulations indeed predict relaxation of the parallel momentum profile from current driven reconnection similar to relaxation of electrical current.³⁵ This work presents first experimental measurements of this phenomenon.

III. MST REVERSED-FIELD PINCH AND DIAGNOSTICS

The RFP is a toroidal plasma confinement configuration similar to a tokamak, but with a relatively weak toroidal magnetic field, which reverses its sign near the plasma edge. The MST RFP has a major plasma radius $R=1.5$ m, and a minor radius $a=0.5$ m.³⁶ The experiments described in this article have been conducted in the regime of relatively low plasma current $I_p=200$ – 250 kA (maximum value achieved in MST is ~ 600 kA), which allowed routine operation of insertable probes at the plasma edge. The other plasma parameters are as follows: the line-averaged plasma density $n \approx 1 \times 10^{13}$ cm⁻³, the reversal parameter, defined as the ratio of the edge to volume-averaged toroidal magnetic field, $F \equiv B_{\phi}(a) / \langle B_{\phi} \rangle_V = -0.2$, and the pinch parameter, defined as the ratio of the edge poloidal field to the volume averaged toroidal field, $\Theta \equiv B_{\theta}(a) / \langle B_{\phi} \rangle_V = 1.7$.

MST plasmas exhibit quasiperiodic relaxation oscillations (sawteeth), illustrated in Fig. 1, with a period of several milliseconds. Sudden bursts of global resistive tearing modes resonant inside the plasma occur at global reconnection events. The bursts are accompanied by the increase in the toroidal magnetic flux [Fig. 1(a)] and rapid change in the core plasma rotation [Fig. 1(b)]. Modes resonant at the reversal surface (with poloidal number $m=0$) are especially prominent [see Fig. 1(d)] and they form a distinct reconnection layer as was established in Ref. 37. This observation has led to the suggestion that fluctuation-induced forces play important role in the current dynamics.

To measure the quantities in Eq. (4) we employ several diagnostics with improved spatial and temporal resolutions. The plasma density profile is measured with a multichord laser interferometer.³⁸ The plasma bulk ion velocity in the core is measured with a Rutherford scattering diagnostic.³⁹ To construct the parallel flow velocity both poloidal and toroidal velocities are needed. Currently, only poloidal measurements are available with the existing Rutherford scattering setup. However, past measurements^{22,24} indicate that the toroidal plasma velocity is very close to the toroidal phase

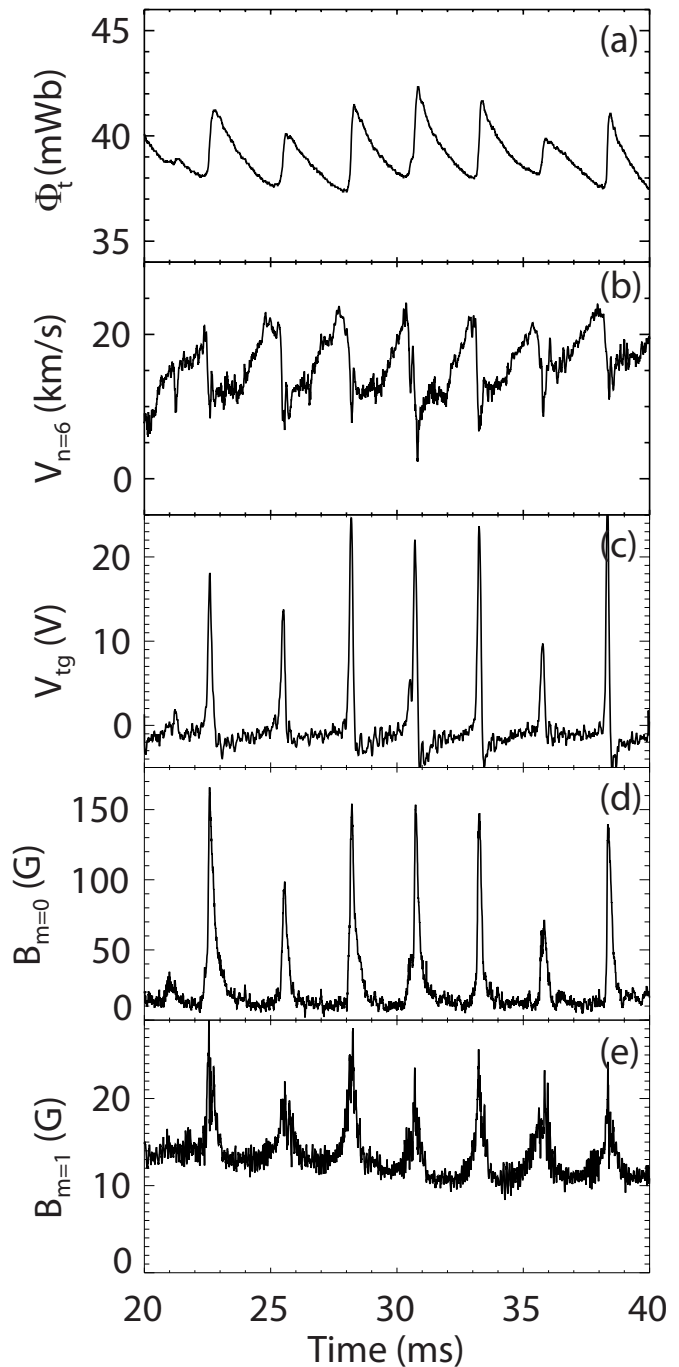


FIG. 1. (Color online) Time traces of the (a) toroidal flux, (b) toroidal velocity of the $m=1, n=6$ core resonant mode, (c) voltage across the toroidal gap in the shell, (d) edge $m=0$ (toroidal modes $1 \leq n \leq 4$) tearing mode amplitude, (e) core $m=1$ (toroidal modes $5 \leq n \leq 15$) tearing mode amplitude measured by the 64-coil edge toroidal array during flat top of the plasma current in the standard MST discharge ($I_p=200$ kA, $F=-0.2$, and $\Theta=1.7$).

velocity of the locally resonant tearing mode. Therefore, the mode rotation velocity, measured with a 64-coil edge toroidal array, is used as a proxy for the toroidal plasma flow in the core.

In addition, we employ several other diagnostics for edge plasma measurements. The poloidal and toroidal components of the bulk plasma flow at the edge are measured by a Mach probe, which consists of four current collectors bi-

ased negatively with respect to a reference tip.⁴⁰ The local radial plasma velocity is measured with an insertable optical (Doppler spectroscopy) probe.⁴¹

The magnetic field is measured with a magnetic probe composed of six magnetic coil triplets separated spatially by 1.65 cm.⁴⁰ The magnetic coils are made from miniature ($\sim 5 \times 3 \times 3$ mm³) chip inductors and have an effective coil area of 9.15 cm². The coils are protected from harsh plasma environment by the boron nitride enclosure. The signals measured by the coils are amplified and integrated to obtain the magnetic field. The overall frequency response of the circuit is ~ 250 kHz, which is sufficient for the accurate measurements of the tearing modes, which frequencies are typically below 50 kHz.

The induced electric field in the edge has been obtained from the poloidal surface loop voltage (toroidal gap voltage) V_{tg} corrected for the flux change inside the torus but outside the radius of the electric field measurement,

$$E_{\parallel}(r) = \frac{V_{tg}}{2\pi r} - \frac{1}{r} \frac{\partial}{\partial t} \int_r^a B_t(r') r' dr'. \quad (6)$$

The contribution of the first term on the RHS is dominant. The equilibrium current density has been determined from Ampere's law by measuring the gradients of the magnetic field,

$$j_{\parallel} = \frac{1}{\mu_0} \left(\frac{1}{R} \frac{\partial B_r}{\partial \phi} - \frac{\partial B_t}{\partial r} \right). \quad (7)$$

IV. OHM'S LAW AND HALL DYNAMO AT THE EDGE

The expression for the Hall dynamo in Eq. (2) can be further simplified by (a) expressing the current density fluctuations using Ampere's law $\mu_0 \tilde{\mathbf{j}} = \nabla \times \tilde{\mathbf{B}}$ and magnetic flux conservation $\nabla \cdot \tilde{\mathbf{B}} = 0$, (b) performing the flux-surface averaging and taking into account that $\partial(\dots)/\partial\theta$ and $\partial(\dots)/\partial\phi$ components of the Maxwell stress (θ -poloidal, ϕ -toroidal directions) vanish after the flux-surface average, and (c) utilizing the fact that the mean magnetic field is primarily in the poloidal direction near the toroidal magnetic field reversal surface. As a result, the parallel component of the Hall dynamo term in the cylindrical coordinates can be expressed as

$$-\frac{1}{ne} \langle \tilde{\mathbf{j}} \times \tilde{\mathbf{B}} \rangle_{\parallel} = -\frac{1}{\mu_0 ne} \left(\frac{\partial}{\partial r} + \frac{2}{r} \right) \langle \tilde{B}_r \tilde{B}_{\theta} \rangle. \quad (8)$$

As can be seen from Eq. (8), evaluation of the Hall dynamo at the edge requires measurements of the correlation product of two fluctuating quantities at two radially separated locations. In the MST edge, this has been accomplished with a magnetic probe as described above.

The temporal variation of the V_{tg} voltage spike across the toroidal gap in the vacuum vessel (one-turn poloidal voltage) during the reconnection events (Fig. 1) provides reference points in time at which the signal reaches its maximum. Correlation analysis has been done relative to these time points and flux-surface averaging has been performed over several hundred reconnection events. Since plasma is rotat-

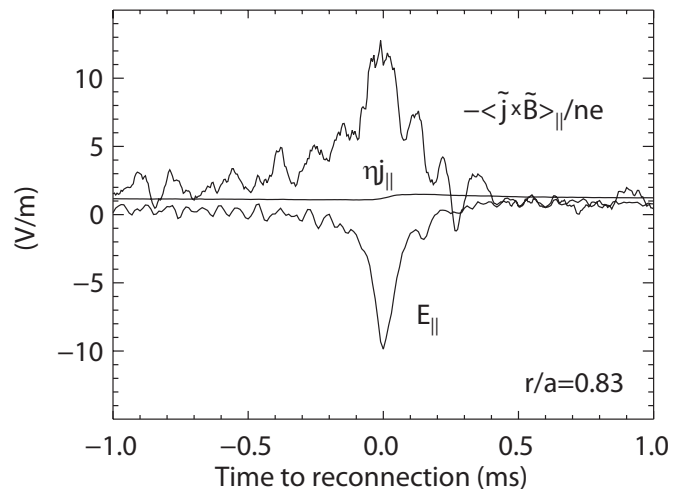


FIG. 2. Ohm's law during a dynamo event cycle near the reversal surface ($r/a=0.83$). The fluctuation-induced Hall dynamo balances the electric field, while change in the ηj_{\parallel} term is small. Rapid oscillations on the time waveforms indicate the uncertainty of the measurements.

ing in the laboratory frame and the reconnection events occur randomly in time, the flux-surface averaging implied in Eq. (2) is equivalent to the conditional averaging over an ensemble of reconnection events, because measurements performed at a single spatial location are randomly distributed over the flux surface.

The time waveforms of the three terms in Ohm's law measured at a radial location $r/a=0.83$ near the toroidal field reversal surface are illustrated in Fig. 2. The $t=0$ moment corresponds to the maximum of the voltage spike at the toroidal gap. The large change in the inductive electric field E_{\parallel} at the reconnection event is balanced by the fluctuation-induced Hall dynamo [Eq. (8)]. The parallel (poloidal) current is generated at the edge during reconnection events, but the change in the resistive term is much smaller than in either the electric field or the Hall dynamo terms. The resistivity is taken to be the classical parallel Spitzer resistivity and is calculated using typical edge plasma parameters: the electron temperature $T_e=30$ eV and the effective charge $Z_{\text{eff}}=2$. During reconnection, the edge current is flowing in the direction opposite to the electric field and is driven by the Hall dynamo. Before the reconnection event, the phase between the radial and poloidal fluctuation components of the magnetic field is close to $\pi/2$ so that the Hall dynamo term is small after flux-surface averaging. At the reconnection event the phase between the radial and poloidal magnetic field components deviates from $\pi/2$ (and the amplitudes of the magnetic fluctuations also increase) which gives rise to the Hall dynamo term.

Figure 3 illustrates the radial profiles of the resistive term $\eta j_{\parallel} - E_{\parallel}$ and the Hall dynamo averaged over 0.15 ms at the peak of the reconnection event. These two terms balance each other near the toroidal magnetic field reversal surface, which is located at $r/a=0.83$, but the balance is violated away from the reversal surface. This result is consistent with previous measurements, suggesting that MHD dynamo is also operating in the plasma edge.¹⁶ The Hall dynamo spatial behavior is opposite to that of the MHD dynamo: It is small

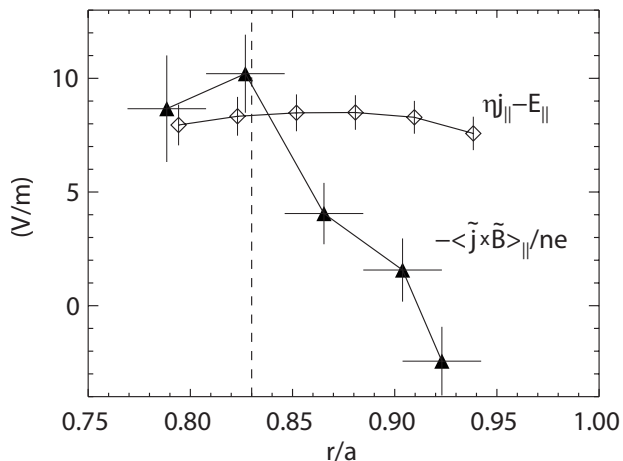


FIG. 3. Edge radial profiles of the resistive term (diamonds) and the Hall dynamo (triangles) averaged over 0.15 ms at the peak of the reconnection event. The dashed line shows the location of the reversal surface.

at the plasma edge and reaches its maximum in the vicinity of the reversal surface where the MHD dynamo vanishes. The spatial extent of the Hall dynamo is of the order of few centimeters, which is consistent with earlier measurements of the Hall dynamo obtained in the core of the MST RFP, near the $q=1/6$ resonant surface.¹⁸

The importance of the two-fluid effects has been also emphasized in a quasilinear calculation of the Hall dynamo, driven by the two-fluid tearing instability, performed in Ref. 17. There, the Hall dynamo term is shown to appear due to zero phase shift between B_r and B_θ in contrast to $\pi/2$ phase in the single-fluid MHD. The Hall dynamo dominates the contribution from the MHD dynamo near the resonant surface in agreement with the experiment. However, the experimental results show a much broader spatial scale for the Hall dynamo than what the quasilinear theory predicts which is likely to indicate the significance of nonlinear dynamics.

V. PARALLEL MOMENTUM TRANSPORT

The time evolution of the parallel plasma velocity at three radial locations through a reconnection event is presented in Fig. 4(a). The initially different parallel flow velocities become nearly equal at the peak of reconnection, which indicates relaxation of the flow profile. The measurements were conditionally averaged over hundreds of reconnection events. The time scale of the relaxation is of the order of 0.1 ms, which is much faster than calculated from collisional viscosity (0.1 s). Similar conclusions were made in earlier experiments^{23,24} investigating momentum transport from externally applied torque.

The parallel momentum $nV_{||}$ exhibits a similar behavior. Figure 4(b) presents the evolution of the radial profile of the parallel momentum normalized by the magnetic field amplitude—Eq. (4). The momentum profile flattening is the most pronounced in the plasma core, while the changes at the edge are small. This is similar to the incomplete relaxation of the parallel current profile observed in these reconnection events.²⁰ Presumably, the strong effect of the boundary con-

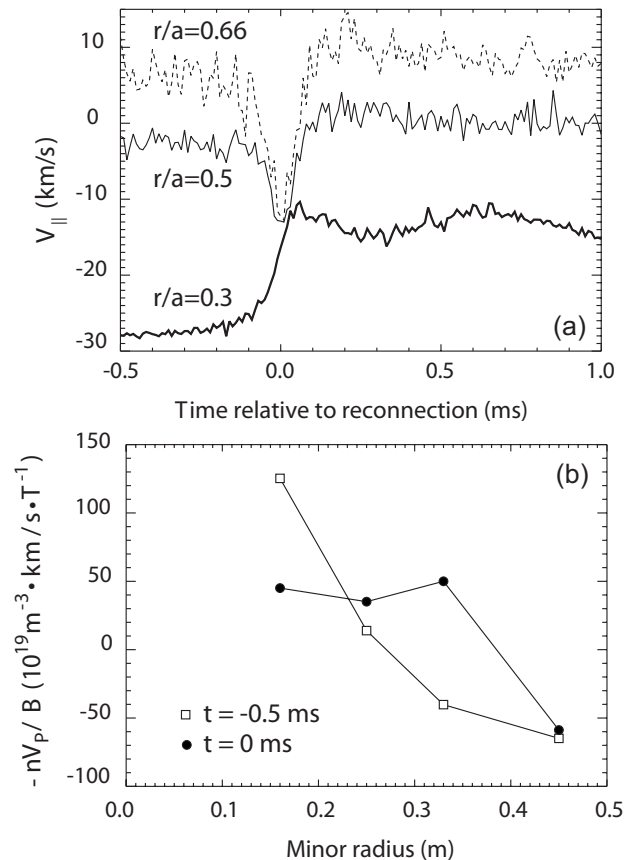


FIG. 4. (a) Parallel velocity at three radial locations. (b) Radial profile of the parallel momentum evolution normalized by the magnetic field before (squares) and during (circles) the reconnection event in MST.

ditions $j_{||}(a)=0$ and $n(a)=0$ that exist in experiment and that are not accounted for by simple relaxation theory plays a role here.

The strong momentum transport observed at the reconnection depends on whether or not nonlinear coupling between the core resonant $m=1$ and edge-resonant $m=0$ tearing modes occurs. This is illustrated in Fig. 5, which shows the change in the core rotation depending on the appearance of a large $m=0$ edge mode. Occasionally, there are events in

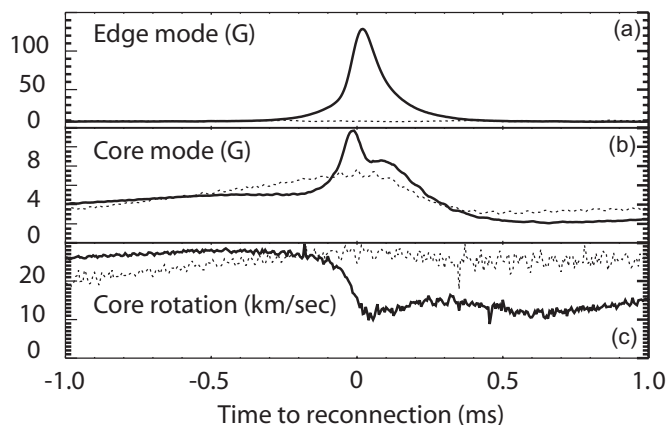


FIG. 5. Amplitudes of (a) edge $m=0$, $n=1$ mode, (b) core $m=1$, $n=6$ mode, and (c) core plasma rotation. When $m=0$ mode is not excited (dashed curves) there is no change in the core plasma rotation.

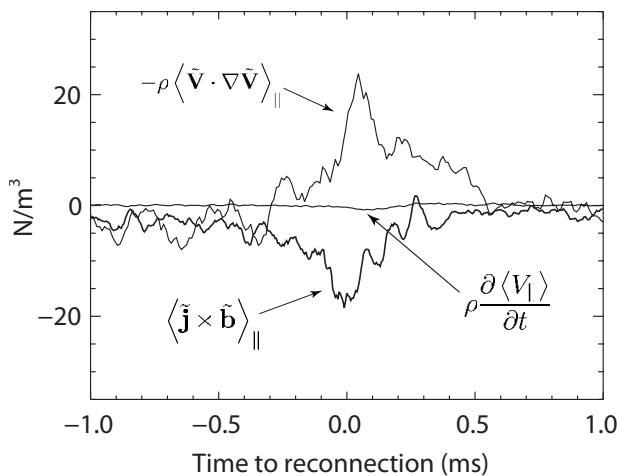


FIG. 6. Parallel momentum balance near the reversal surface ($r/a=0.83$) through the reconnection event. Rapid oscillations on the data curves indicate experimental uncertainty.

which only the $m=1$ mode grows, but the $m=0$ mode amplitude remains small (dashed curves). The momentum transport is observed to be large only when both the $m=1$ and $m=0$ modes grow to large amplitudes (solid curves). These results further extend an earlier observation that momentum transport is small in the nonreversed plasma discharges without the edge-resonant $m=0$ mode.²³

The expressions for the fluctuation-induced stresses can be simplified to be made more suitable for measurements. Using the procedure described in the Sec. IV [Eq. (8)], the parallel (poloidal at the RFP edge) component of the Maxwell stress in the cylindrical approximation can be represented as $\langle \tilde{\mathbf{j}} \times \tilde{\mathbf{B}} \rangle_{||} = 1/\mu_0 (\partial/\partial r + 2/r) \langle \tilde{B}_r \tilde{B}_\theta \rangle$, and the Reynolds stress as $\langle \tilde{\mathbf{V}} \cdot \nabla \tilde{\mathbf{V}} \rangle_{||} = (\partial/\partial r + 2/r) \langle \tilde{V}_r \tilde{V}_\theta \rangle$. The expression for the Reynolds stress is derived under an assumption of flow incompressibility $\nabla \cdot \mathbf{V} = 0$. This assumption is widely used for tearing modes and is confirmed through numerical simulations. The radial derivative in the Maxwell stress was calculated in a single shot utilizing the radially separated magnetic triplets. For the Reynolds stress, the optical and the Mach probes were moved radially between shots.

The time evolution of all three terms in Eq. (5) measured at the toroidal field reversal surface ($r/a=0.83$) is shown in Fig. 6. The Maxwell and Reynolds stresses are individually large and approximately balance each other with a difference in the order of the ion inertia term. The same behavior is observed at all radii across the plasma edge region—Fig. 7.

VI. DISCUSSION

The experimental observations exhibit many similarities with analytical findings and numerical simulations.³⁵ In particular, it is observed in numerical simulations that momentum transport is greatly enhanced in the presence of multiple tearing modes. It has been also observed that the effect of multiple, nonlinearly coupled tearing modes is not merely the superposition of independent, radially separated resonant modes. The nonlinear mode coupling leads to the change in the phase between the fluctuation quantities in the Maxwell

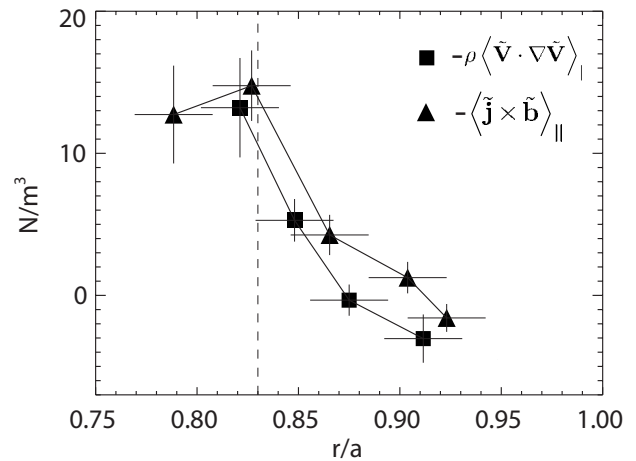


FIG. 7. Radial profiles of the Maxwell (triangles) and Reynolds (squares) stresses averaged over 0.15 ms at the peak of the reconnection event. The dashed line marks the toroidal magnetic field reversal surface.

and Reynolds stresses, therefore strengthening the turbulent stresses. Artificial suppression of the $m=0$ mode in computations leads to the suppression of the nonlinear coupling. In this case the plasma evolves to a quasi-steady-state without sawtooth oscillations and momentum transport is greatly reduced, much like in the experiment.

The measurements performed at the MST edge are consistent with the measurements in the core. The Maxwell stress is measured by laser Faraday rotation,⁴² which is capable of measuring magnetic fluctuations. It is observed that the Maxwell stress in the core is much larger than the inertial term (Fig. 8). The Reynolds stress has not yet been measured in the core. It has also been shown that the Hall dynamo, which is directly related to the Maxwell stress, balances the parallel electric field during reconnection in the core. The reason for the strong increase of the Hall dynamo at the reconnection event has been attributed to the change of the phase between the current density and magnetic field fluctuations due to nonlinear mode coupling.^{18,19}

The observation that the individual fluctuation-induced Maxwell and Reynolds stresses are much larger than the ion inertia is somewhat surprising. The reason might be related to the above mentioned coupling of the momentum transport to the current density transport. This coupling stems from the common fluctuation-induced Lorentz force entering both the

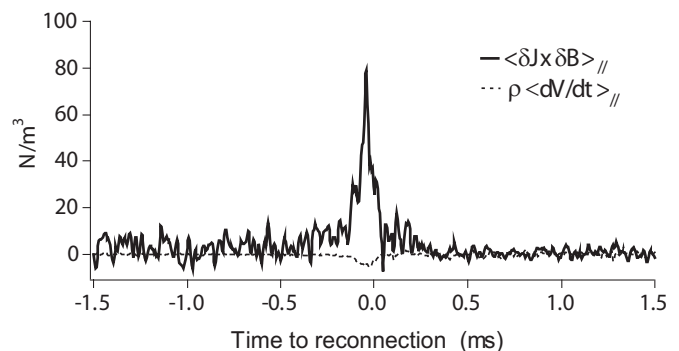


FIG. 8. Time evolution of the Maxwell stress (solid line) and ion inertia (dashed line) in the plasma core.

momentum balance equation (as Maxwell stress) and Ohm's law (as Hall dynamo). Thus, a large Hall dynamo (that relaxes the current density profile) would also produce a strong effect on plasma momentum. If the plasma has a preferred flow profile (e.g., mandated by flow effects on tearing instability), then a strong, opposing Reynolds stress would need to arise. Work is in progress to reproduce the interplay between the two large fluctuation-induced stresses through two-fluid MHD simulations, including the resistivity and viscosity that match the experiment.

VII. CONCLUSIONS

In summary, rapid parallel momentum transport from current driven tearing instability is observed in the MST RFP. It is established that tearing modes transport momentum and that the transport is strongly enhanced through nonlinear mode coupling. The Maxwell and Reynolds stresses are measured by probes in the edge and are found to be individually large, but oppositely directed, with the difference in the order of the ion inertia. The Hall dynamo has been also measured in the edge and balances the parallel electric field in Ohm's law. The momentum dynamics is shown to be closely coupled to the current dynamics. The Maxwell stress enters the parallel Ohm's law in the vicinity of the resonant surfaces (as the Hall dynamo) and drives the parallel current profile relaxation. This mechanism could play a role in tokamaks during periods of strong MHD activity. In addition, these results have connections to astrophysics. For example, considerable momentum transport is expected to exist in accretion disks formed around black holes. Momentum transport from current-driven tearing instability can be an alternative to the standard theory of transport from flow-driven magnetorotational instability.

ACKNOWLEDGMENTS

The authors would like to acknowledge insightful discussions with D. Craig, F. Ebrahimi, and T. D. Tharp and would like to thank members of the MST group for technical assistance. This work was supported by the U.S. DOE (Contract No. DE-FC02-05ER54814) and NSF (Contract No. PHY-0215581).

¹For example, J. E. Rice, A. Ince-Cushman, J. S. deGrassie, L.-G. Eriksson, Y. Sakamoto, A. Scarabosio, A. Bortolon, K. H. Burrell, B. P. Duval, C. Fenzi-Bonizic, M. J. Greenwald, R. J. Groebner, G. T. Hoang, Y. Koide, E. S. Marmor, A. Pochelon, and Y. Podpaly, *Nucl. Fusion* **47**, 1618 (2007).

²Ö. Gürçan, P. Diamond, T. Hahm, and R. Singh, *Phys. Plasmas* **14**, 042306 (2007).

³V. Antoni, E. Spada, N. Vianello, M. Spolaore, R. Cavazzana, G. Serianni, and E. Martines, *Plasma Phys. Controlled Fusion* **47**, B13 (2005).

⁴N. Vianello, E. Spada, V. Antoni, M. Spolaore, G. Serianni, G. Regnoli, R. Cavazzana, H. Bergsaker, and J. R. Drake, *Phys. Rev. Lett.* **94**, 135001 (2005).

⁵S. A. Balbus and J. F. Hawley, *Astrophys. J.* **376**, 214 (1991).

⁶A. B. Rechester and M. N. Rosenbluth, *Phys. Rev. Lett.* **40**, 38 (1978).

⁷S. C. Prager, *Plasma Phys. Controlled Fusion* **32**, 903 (1990).

⁸G. Fiksel, R. D. Bengtson, M. Cekic, D. Den Hartog, S. C. Prager, P. Pribyl, J. Sarff, C. Sovinec, M. R. Stoneking, R. J. Taylor, P. W. Terry, G. R. Tynan, and A. J. Wootton, *Plasma Phys. Controlled Fusion* **38**, A213 (1996).

⁹R. J. Bickerton, *Plasma Phys. Controlled Fusion* **39**, 339 (1997).

¹⁰S. Assadi, S. C. Prager, and K. L. Sidikman, *Phys. Rev. Lett.* **69**, 281 (1992).

¹¹S. Choi, D. Craig, F. Ebrahimi, and S. C. Prager, *Phys. Rev. Lett.* **96**, 145004 (2006).

¹²S. Gangadhara, D. Craig, D. A. Ennis, D. J. D. Hartog, G. Fiksel, and S. C. Prager, *Phys. Plasmas* **15**, 056121 (2008).

¹³S. Ortolani and D. D. Schnack, *Magnetohydrodynamics of Plasma Relaxation* (World Scientific, Singapore, 1993).

¹⁴H. Ji, S. C. Prager, A. F. Almagri, J. S. Sarff, Y. Yagi, Y. Hirano, K. Hattori, and H. Toyama, *Phys. Plasmas* **3**, 1935 (1996).

¹⁵D. J. Den Hartog, J. T. Chapman, D. Craig, G. Fiksel, P. W. Fontana, S. C. Prager, and J. S. Sarff, *Phys. Plasmas* **6**, 1813 (1999).

¹⁶P. W. Fontana, D. J. Den Hartog, G. Fiksel, and S. C. Prager, *Phys. Rev. Lett.* **85**, 566 (2000).

¹⁷V. V. Mirnov, C. C. Hegna, and S. C. Prager, *Plasma Phys. Rep.* **29**, 566 (2003).

¹⁸W. X. Ding, D. L. Brower, D. Craig, B. H. Deng, G. Fiksel, V. V. Mirnov, S. C. Prager, J. S. Sarff, and V. Svidzinski, *Phys. Rev. Lett.* **93**, 045002 (2004).

¹⁹W. X. Ding, D. L. Brower, B. H. Deng, A. F. Almagri, D. Craig, G. Fiksel, V. V. Mirnov, S. C. Prager, J. S. Sarff, and V. Svidzinski, *Phys. Plasmas* **13**, 112306 (2006).

²⁰D. L. Brower, W. X. Ding, S. D. Terry, J. K. Anderson, T. M. Biewer, B. E. Chapman, D. Craig, C. B. Forest, S. C. Prager, and J. S. Sarff, *Phys. Rev. Lett.* **88**, 185005 (2002).

²¹S. D. Terry, D. L. Brower, W. X. Ding, J. K. Anderson, T. M. Biewer, B. E. Chapman, D. Craig, C. B. Forest, R. O'Connell, S. C. Prager, and J. S. Sarff, *Phys. Plasmas* **11**, 1079 (2004).

²²D. J. Den Hartog, A. F. Almagri, J. T. Chapman, H. Ji, S. C. Prager, and J. S. Sarff, *Phys. Plasmas* **2**, 2281 (1995).

²³A. K. Hansen, A. F. Almagri, D. Craig, D. J. Den Hartog, C. C. Hegna, S. C. Prager, and J. S. Sarff, *Phys. Rev. Lett.* **85**, 3408 (2000).

²⁴A. F. Almagri, J. T. Chapman, C. S. Chiang, D. Craig, D. J. Den Hartog, C. C. Hegna, and S. C. Prager, *Phys. Plasmas* **5**, 3982 (1998).

²⁵J. B. Taylor, *Phys. Rev. Lett.* **33**, 1139 (1974).

²⁶J. K. Anderson, T. M. Biewer, C. B. Forest, R. O'Connell, S. C. Prager, and J. S. Sarff, *Phys. Plasmas* **11**, L9 (2004).

²⁷L. Spitzer, Jr., *Physics of Fully Ionized Gases*, 2nd revised ed. (Interscience, New York, 1962), p. 28.

²⁸T. Terasawa, *Geophys. Res. Lett.* **10**, 475, DOI:10.1029/GL010i006p00475 (1983).

²⁹J. Birn, J. F. Drake, M. A. Shay, B. N. Rogers, R. E. Denton, M. Hesse, M. Kuznetsova, Z. W. Ma, A. Bhattacharjee, A. Otto, and P. L. Pritchett, *J. Geophys. Res.* **106**, 3715, DOI:10.1029/1999JA900449 (2001).

³⁰A. Vaivads, Y. Khoyaintsev, M. Andre, A. Retino, S. C. Buchert, B. N. Rogers, P. Decreau, G. Paschmann, and T. D. Phan, *Phys. Rev. Lett.* **93**, 105001 (2004).

³¹M. Yamada, Y. Ren, H. Ji, J. Breslau, S. Gerhardt, R. Kulsrud, and A. Kuritsyn, *Phys. Plasmas* **13**, 052119 (2006).

³²H. Ji, A. F. Almagri, S. C. Prager, and J. S. Sarff, *Phys. Rev. Lett.* **73**, 668 (1994).

³³L. C. Steinhauer and A. Ishida, *Phys. Rev. Lett.* **79**, 3423 (1997).

³⁴C. C. Hegna, *Phys. Plasmas* **5**, 2257 (1998).

³⁵F. Ebrahimi, V. V. Mirnov, S. C. Prager, and C. R. Sovinec, *Phys. Rev. Lett.* **99**, 075003 (2007).

³⁶R. N. Dexter, D. W. Kerst, T. W. Lovell, S. C. Prager, and J. C. Sprott, *Fusion Technol.* **19**, 131 (1991).

³⁷N. A. Crocker, G. Fiksel, S. C. Prager, and J. S. Sarff, *Phys. Rev. Lett.* **90**, 035003 (2003).

³⁸N. E. Lanier, D. Craig, J. K. Anderson, T. M. Biewer, B. E. Chapman, D. J. Den Hartog, C. B. Forest, S. C. Prager, D. L. Brower, and Y. Jiang, *Phys. Plasmas* **8**, 3402 (2001).

³⁹J. C. Reardon, G. Fiksel, C. B. Forest, A. F. Abdrashitov, V. I. Davydenko, A. A. Ivanov, S. A. Korepanov, S. V. Murachtin, and G. I. Shulzhenko, *Rev. Sci. Instrum.* **72**, 598 (2001).

⁴⁰A. Kuritsyn, G. Fiksel, A. F. Almagri, M. Miller, M. Reyfman, and J. S. Sarff, *Rev. Sci. Instrum.* **79**, 10F127 (2008).

⁴¹A. Kuritsyn, D. Craig, G. Fiksel, M. Miller, D. Cylinder, and M. Yamada, *Rev. Sci. Instrum.* **77**, 10F112 (2006).

⁴²W. X. Ding, D. L. Brower, B. H. Deng, D. Craig, S. C. Prager, and V. Svidzinski, *Rev. Sci. Instrum.* **75**, 3387 (2004).